

See discussions, stats, and author profiles for this publication at: <https://www.researchgate.net/publication/265794169>

Aspect Ratio Effect on Multiple Flow Solutions in a Two-Sided Parallel Motion Lid-Driven Cavity

Article in JOURNAL OF MECHANICS · October 2014

CITATIONS

0

READS

75

1 author:



[Win-jet Luo](#)

National Chin-Yi University of Technology

77 PUBLICATIONS 258 CITATIONS

[SEE PROFILE](#)



Aspect Ratio Effect on Multiple Flow Solutions in a Two-Sided Parallel Motion Lid-Driven Cavity

K.-T. Chen, C.-C. Tsai, W.-J. Luo, C.-W. Lu and C.-H. Chen

Journal of Mechanics / *FirstView* Article / September 2014, pp 1 - 8
DOI: 10.1017/jmech.2014.51, Published online: 12 August 2014

Link to this article: http://journals.cambridge.org/abstract_S1727719114000513

How to cite this article:

K.-T. Chen, C.-C. Tsai, W.-J. Luo, C.-W. Lu and C.-H. Chen Aspect Ratio Effect on Multiple Flow Solutions in a Two-Sided Parallel Motion Lid-Driven Cavity. Journal of Mechanics, Available on CJO 2014 doi:10.1017/jmech.2014.51

Request Permissions : [Click here](#)

ASPECT RATIO EFFECT ON MULTIPLE FLOW SOLUTIONS IN A TWO-SIDED PARALLEL MOTION LID-DRIVEN CAVITY

K.-T. Chen C.-C. Tsai

*Department of Applied Mathematics
National Chung Hsing University
Taichung, Taiwan*

W.-J. Luo *

*Graduate Institute of Precision Manufacturing
National Chin-Yi University of Technology
Taichung, Taiwan*

C.-W. Lu

*Department of Refrigeration, Air Conditioning and Energy Engineering
National Chin-Yi University of Technology
Taichung, Taiwan*

C.-H. Chen

*Department of Mechanics
National Chin-Yi University of Technology
Taichung, Taiwan*

ABSTRACT

A continuation method, accompanied with a linear stability analysis, is employed to investigate the bifurcation diagram of the flow solutions, as well as the multiple flow states in a cavity with different aspect ratios for parallel motion of two facing lids. The Reynolds number proportional to the wall velocity is used as the continuation parameter, and the evolution of the bifurcation diagrams in cases with different aspect ratios is illustrated. The induced flow patterns are highly dependent upon both the aspect ratios and the moving velocity of the walls. Three different types of bifurcation diagrams and their corresponding flow states are classified according to the aspect ratios. One stable symmetric flow state and one stable asymmetric flow state are identified. The stable asymmetric flow state is obtained at a high aspect ratio and a low Reynolds number. Meanwhile, the regions of stable and unstable flows are distinguished according to the different aspect ratios.

Keywords: Instabilities, Flow bifurcation, Lid-driven cavity flow, Aspect ratio.

1. INTRODUCTION

Cavity flow driven by moving boundaries is not only technically important, but also of great scientific interest. Although the problem seems simple, it reveals the complex phenomena of vortex dynamics, hydrodynamic stability, flow bifurcation, *etc.* Cavity flow was often found in certain engineering applications, such as short-dwell coating, removal of species from structured surfaces and mixing and flow in drying devices, and was studied in academic research as well. Classic cavity flows are usually driven by either one-sided or two-sided facing lids moving in tangential directions. One-sided lid-driven cavity flow has been extensively studied in literature [1-4].

For the two-sided lid-driven cavity flow which is induced by two facing sides moving with the same velocities in opposite directions to each other, Kuhlmann *et al.* [5,6] employed experimental and theoretical methods to investigate the induced two and three-dimensional flows in the cavity, and found that the existence of multiple two-dimensional steady flows depends upon the cavity aspect ratio and the wall driving velocities. Albensoeder *et al.* [7] used a numerical method to investigate the two-sided lid-driven cavity

flows, and identified the stability of the found non-unique steady flows. Alleborn *et al.* [8] investigated a two-dimensional flow in a two-sided lid-driven cavity in which a temperature gradient was established and thermal transport was generated. Albensoeder and Kuhlmann [9] performed a linear stability analysis to show that the two-dimensional flow becomes unstable in different modes, depending on the cross-sectional aspect ratio and Reynolds number. Blohm and Kuhlmann [10] employed Laser-Doppler and hot-film techniques to measure steady and time-dependent vortex flows which occur at higher Reynolds numbers. Yang and Luo [11] investigated the multiple two-dimensional steady flow solutions in the cavity flow with heat transport and the flow transitions between the found stable solutions; they established a thumb-shaped boundary line which identifies a restricted region of a stable solution in terms of the Grashof and Reynolds numbers.

Albensoeder and Kuhlmann [12] employed linear stability to investigate the flows driven by the parallel motion of two facing walls in a rectangular cavity by a finite volume method, in order to establish critical curves in terms of the critical Reynolds number on the aspect ratio. The results indicated that, while the two

* Corresponding author (wjluo@ncut.edu.tw)

facing sides of the cavity move with constant velocities in the same direction, a stable two-vortex flow can be induced, in which the vortices adjacent to the upper and bottom walls of the cavity rotate, respectively, in clockwise and counterclockwise directions. With the variation of the Reynolds number, the symmetry of the two-vortex flow state can be broken via the symmetry-breaking bifurcation points, and a stable asymmetric flow state formed.

Recently, Chen *et al.* [13] investigated the flow bifurcations in a two-sided lid-driven cavity with different aspect ratios for anti-parallel motion by the continuation method. The evolution of the bifurcation diagrams in cases with different aspect ratios was illustrated. Two stable symmetric flows and one stable asymmetric flow were identified, and the regions of the stable flows in the aspect ratios and Reynolds numbers were distinguished. Cadou *et al.* [14] investigated the flow bifurcations in the two-sided non-facing lid-driven cavity and the four-sided lid-driven cavity, respectively. The critical value of the pitchfork bifurcations and hopf bifurcation were identified. Waheed [15] investigated the fluid flow and heat transfer induced by a lid driving force and a buoyancy force resulting from the temperature gradient on the vertical walls within rectangular enclosures. Noor, Kanna and Chern [16] numerically investigated the flow and heat transfer inside a square cavity with double-sided oscillating lids; they showed four different flow patterns at different frequencies for Reynolds numbers greater than 300.

In a systematic study on the respective instabilities and nonlinear pattern formations, the basic two-dimensional flow solutions' dependence on the critical Reynolds number and the aspect ratio proved difficult to determine. In this study, the nonlinear steady Navier-Stokes equations were solved by following the so-called continuation method [17]. This approach was often applied to search for possible stable and unstable steady-state solutions and to construct bifurcation diagrams for different aspect ratios. Thus, the purpose of the present study was to systematically illustrate the stability of the two-dimensional solution manifold of such flows with different Reynolds numbers and aspect ratios. The evolution of the bifurcation diagrams, in terms of Reynolds numbers with aspect ratios, is presented and the regions of the stable flows in the aspect ratios and Reynolds numbers, distinguished.

2. NUMERICAL ASPECT

2.1 Governing Equations

Figure 1 presents the geometric model and corresponding boundaries of a cavity whose height and width are signified by H and L , respectively, and with an incompressible Newtonian fluid filled within the cavity. In the study, the aspect ratio (AR) of the cavity is defined as H/L . The upper and lower walls move at the same velocity of U_b in the right direction. The stationary vertical walls are considered to be solid and adiabatic.

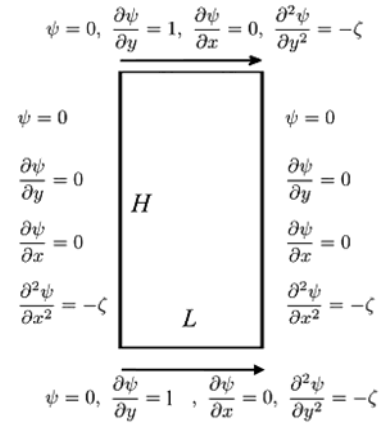


Fig. 1 Schematic illustration of the cavity and its corresponding boundary conditions.

Dimensionless governing equations for the stream function (ψ) and vorticity function (ζ), respectively, can be written as [11]:

$$\frac{\partial^2 \psi}{\partial x^2} + \frac{\partial^2 \psi}{\partial y^2} = -\zeta, \quad (1)$$

$$\frac{\partial \zeta}{\partial t} + \frac{\partial \psi}{\partial y} \frac{\partial \zeta}{\partial x} - \frac{\partial \psi}{\partial x} \frac{\partial \zeta}{\partial y} = \frac{1}{Re} \left(\frac{\partial^2 \zeta}{\partial x^2} + \frac{\partial^2 \zeta}{\partial y^2} \right), \quad (2)$$

where $Re = U_b L / \nu$ is the Reynolds number and ν is the kinematic viscosity of the fluid.

The boundary conditions of the cavity flow used in the numerical calculations are expressed as follows:

On the top wall ($y = H/L$):

$$\psi = 0, \quad \frac{\partial \psi}{\partial y} = 1, \quad \frac{\partial^2 \psi}{\partial y^2} = -\zeta.$$

On the bottom wall ($y = 0$):

$$\psi = 0, \quad \frac{\partial \psi}{\partial y} = 1, \quad \frac{\partial^2 \psi}{\partial y^2} = -\zeta.$$

On the left-side wall ($x = 0$):

$$\psi = 0, \quad \frac{\partial \psi}{\partial x} = 0, \quad \frac{\partial^2 \psi}{\partial x^2} = -\zeta.$$

On the right-side wall ($x = 1$):

$$\psi = 0, \quad \frac{\partial \psi}{\partial x} = 0, \quad \frac{\partial^2 \psi}{\partial x^2} = -\zeta.$$

The flow is driven by the upper and lower cavity walls, which move with equal velocity towards the right. Thus, the right-moving direction of the walls causes $\partial \psi / \partial y = 1$ in conditions (a) and (b). Note that the tangential derivatives of ψ on the boundaries are not used in the computation since it suffices to set $\psi = 0$. To establish the steady solution manifold of the cavity flow, it is first necessary to drop the $\partial \zeta / \partial t$ term from (2).

2.2 Numerical Method

The governing Eqs. (1) and (2) are discretized by central differences of a second order in an irregular grid system, and a system of non-linear algebraic equations is formed,

$$i.e. G(X, \lambda) = 0, \quad (3)$$

where X is the solution vector and λ is the continuation parameter, which is the Reynolds number in this study.

This then gives an iterative sequence, $[X^{(v)}(\lambda)]$, which is expressed as:

$$X^{(0)}(\lambda) \equiv \text{initial estimate}, \quad (4a)$$

$$G_X(X^{(v)}(\lambda)) [X^{(v+1)} - X^{(v)}] = -G(X^{(v)}, \lambda), \quad v = 0, 1, 2, \dots, \quad (4b)$$

where G_X is the Jacobian matrix of Eq. (3). When $\lambda = 0$ a solution of the continuous problem can be obtained by numerical methods. As λ deviates from zero, we can use the solution as an initial estimate of the discrete solution in the Euler-Newton method applied to Eq. (4). One way to obtain good initial estimates in the iterative sequence of Eq. (4) is to use a Taylor expansion of the solution with respect to changes in parameter λ :

$$X(\lambda + \delta\lambda) = X(\lambda) + \delta\lambda X_\lambda(\lambda). \quad (5a)$$

To obtain X_λ , we can use Eq. (3) and it satisfies:

$$G_\lambda(X, \lambda) = -G_X(X, \lambda)X_\lambda. \quad (5b)$$

The iterative method as described in Eqs. (4) and (5) is known as the Euler-Newton continuation. In the study, the basic state solution was obtained by central differences of a second order in the irregular grid system, but a minimum value of the continuation parameter was substituted into the iteration of Eqs. (4) ~ (5) in order to successfully attain a converging solution. This method is extremely effective and usually converges quadratically; however, the method fails at points where the Jacobian matrix $G_X(X, \lambda) = 0$ is singular. To avoid the singular points, the continuation method (Keller [17], Yang [20]) was introduced:

$$N(X(s), \lambda(s)) \equiv \dot{X}(s_0) \cdot [X(s) - X(s_0)] + \dot{\lambda}(s_0) [\lambda(s) - \lambda(s_0)] - (s - s_0) = 0, \quad (6)$$

where $[X(s_0), \lambda(s_0)]$ is a previously computed solution for λ and $s = s_0$. $\dot{X} = dX/ds$ and $\dot{\lambda} = d\lambda/ds$ denote the components of a tangent vector to the solution path $[X(s), \lambda(s)]$.

A new system of equations can then be written as:

$$\begin{cases} G(X, \lambda) = 0 \\ N(X, \lambda, s) = 0 \end{cases}$$

The Jacobian matrix of this new system is given as follows:

$$\frac{\partial(G, N)}{\partial(X, \lambda)} = \begin{pmatrix} G_X & G_\lambda \\ N_X & N_\lambda \end{pmatrix}. \quad (7)$$

with the Euler-Newton continuation in parameter s rather than in λ , it is also possible to follow the solution around singular points.

A linear stability analysis was performed in order to investigate the stability of the various flow states obtained by the continuation method described above. The basic state, X_0 , identified by Newton's method during continuation is perturbed by small, time-dependent quantities:

$$X = X_0 + \varepsilon e^{\gamma t}, \quad (8)$$

where ε is a small disturbance vector.

For transient solutions, a set of time-dependent equations can be derived and expressed as:

$$M(X) \frac{dX}{dt} = G(X, \lambda), \quad (9)$$

where $M(X)$ is the mass matrix. This matrix is singular because some equations, *e.g.* the equations for stream function, do not possess an explicit time-dependent term. Substituting Eq. (8) into Eq. (9), after collecting the linear terms of ε , gives the generalized algebraic eigenvalue problem:

$$\gamma M(X_0) \varepsilon = \tilde{J}(X_0) \varepsilon, \quad (10)$$

where the matrix \tilde{J} represents the Jacobian matrix of $G(X, \lambda)$ evaluated for a basic state solution.

The stability characteristics of the basic state, X_0 , are determined by the sign of the eigenvalue, γ . The basic solution is infinitesimally stable if $\text{Re}\{\gamma\} < 0$ holds for all eigenvalues, γ , *i.e.*, if all perturbations in Eq. (8) decay with time. However, if at least one eigenvalue exists for the case where $\text{Re}\{\gamma\} > 0$, the corresponding eigenmode will grow, as $t \rightarrow \infty$, and the basic solution will be unstable. However, because M is singular, some eigenvalues are infinite and do not contribute to linear instability. When calculating the leading eigenvalues, it is necessary to remove these infinite eigenvalues. An effective algorithm for doing so is the shift-and-inverse Arnoldi operation (Sorensen [18]). The generalized eigenvalue problem given in Eq. (10) can be transformed into a standard eigenvalue problem as follows:

$$(\tilde{J} - \beta M)^{-1} M \varepsilon = \hat{\gamma} \varepsilon, \quad \hat{\gamma} = \frac{1}{\gamma - \beta} \quad (11)$$

where β is a complex shift parameter such that $[(\tilde{J} - \beta M)^{-1} M]$ is not singular.

This standard problem is then solved by a restarted, iterative Arnoldi method, which is essentially a sophisticated extension of the power iteration method, and which allows a number of eigenvalues, $\hat{\gamma}$, of largest magnitude to be calculated via ARPACK (Saad [19]). For the detailed algorithm of the linear stability analysis, one can refer to the studies of Yang and Luo [20], Luo *et al.* [21] and Chen *et al.* [13].

3. RESULTS AND DISCUSSION

Two-dimensional steady incompressible flows in a rectangular cavity with aspect ratios (AR) ranging from 0.5 to 1.0 for Reynolds numbers from 0 to 2000, were calculated. The flow was driven by parallel moving walls, which moved with equal velocity in the same tangential direction. The Reynolds number defined in this study was proportional to the moving velocities of the walls. For this kind of cavity flow, Altensoeder *et al.* [9] indicated that the existent range of asymmetric flow was between aspect ratios greater than 0.5 and less than 1.1 for Reynolds numbers lower than 2000; thus, the range of aspect ratio ($0.5 < AR < 1$) was chosen. After grid independent analysis, non-equal space grid points of 91×151 stretching from all boundaries were employed for all calculations by continuation method.

3.1 Three Different Types of Flow Bifurcation in Flows with Aspect Ratios in the Calculated Range

Flow bifurcation in the aspect ratio range of 0.5 to 1 can be classified according to three different types depending on the patterns of the corresponding bifurcations. The first type of flow bifurcation is similar to that shown in Fig. 2, which plots the value of the stream function at the cavity center with the aspect ratio of 0.57 as a function of the Reynolds number. Five segments are identified and the corresponding streamline contours of the flow patterns are illustrated in Fig. 2. In this figure, the symbols “+” and “-” denote the flow state on each segment being stable or unstable, respectively. However, the labels “S” and “A” indicate that the flow patterns on the segments are symmetric and asymmetric to the horizontal center line of the cavity, respectively. The stable two-vortex flow state (+S₁) is comprised of two symmetrical counter-rotating vortices in the upper and lower half regions existing in the range of $Re = 0$ to $Re = 535$. Along segment (+S₁), the flow states were stable until point P₁, which represents a symmetry-breaking point at $Re = 535$. After point P₁, segment (+S₁) is divided into three separate segments: (+A₁), (+A₂) and (-S₂). Flows in segments (+A₁) and (+A₂) inherited the stable flow characteristics evidently in segment (+S₁) and exhibited an asymmetric state, while the flow in segment (-S₂) exhibited an unstable state which persisted until point P₂ ($Re = 1590$), at which another symmetry-breaking bifurcation point was identified. Along segments (+A₁) and (+A₂), the asymmetry of the flow was gradually augmented, and then decreased quickly with the increased Reynolds number. When the Reynolds number was greater than 1590, only one stable symmetric state (+S₃) existed in the range.

Along the continuation path from segments (+S₁), (-S₂) and (+S₃), two separate vortices appeared adjacent to each of the moving walls in the flow patterns. The vortices adjacent to the upper and bottom walls of the cavity rotated in clockwise and counterclockwise directions, respectively, and their strength increased as the Reynolds number rose. This flow pattern is referred to as a two-vortex flow.

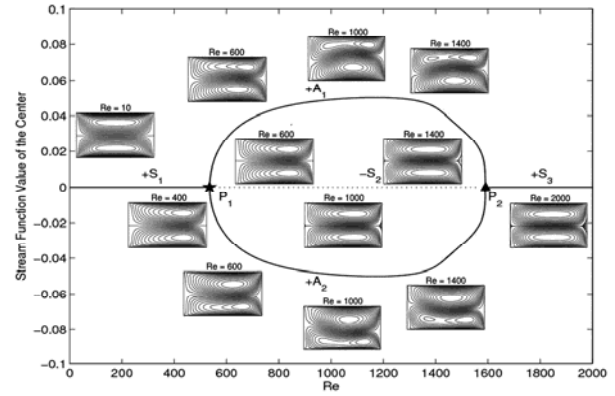


Fig. 2 Stream function values at the cavity center traced by Reynolds number and the corresponding flow states for the case with $AR = 0.57$.

Figure 3 illustrates the flow evolution of the flow states along the continuation path of segment (+A₁). Along the segment, the lower vortex adjacent to the lower wall grew in size and strength, causing the other vortex to shrink in size with the increased Reynolds number, and a stable asymmetric flow state formed. The asymmetry of the asymmetric flows originating from the symmetry-breaking bifurcation point P₁ gradually increased with the increased Reynolds number. When the Reynolds number was equal to 1170, the asymmetry of the flow state reached its maximum value. Then, the upper small vortex adjacent to the upper wall quickly grew in size and strength, and compressed the lower larger vortex so that it shrank in size. At point P₂, the flow state returned to a stable symmetric flow. The flow state along segment (+A₂) was similar to that of segment (+A₁); however, the flow patterns of the same Reynolds number in the two segments were symmetric to the horizontal center line of the cavity.

The second type of flow bifurcation is similar to that shown in Fig. 4, which plots the value of the stream function at the cavity center as a function of the Reynolds number for a two-sided parallel lid-driven cavity flow with AR equal to 0.877. Nine segments are identified in the flow bifurcation diagram.

Along segment (+S₁), the flow was symmetric and stable for a Reynolds number less than 594. As the Reynolds number increased, the strength of the vortices also increased. At the pitchfork bifurcation point, P₁ ($Re = 594$), segment (+S₁) was divided into three separate segments: (-A₁), (-A₂) and (-S₂). Along segment (-S₂), the flow of the two vortices was symmetric, but it destabilized via P₁. Then, with the increase in Reynolds number, the symmetric flow of the two vortices was stabilized again by the second bifurcation point, P₂ ($Re = 641$). However, along segments (-A₁) and (-A₂), the flow states were also destabilized by bifurcation point P₁ and became unstable asymmetric flows with the decreased Reynolds number. Then, by the turning points, T₁ and T₂ at $Re = 504$, the asymmetric flows stabilized again, respectively. With the increased Reynolds number, one of the two vortices grew

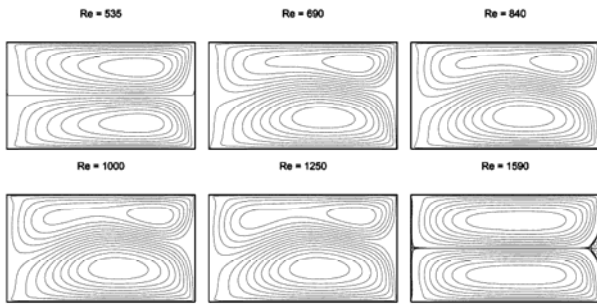


Fig. 3 Asymmetric flow patterns for parallel motion along $+A_1$ with $AR = 0.57$.

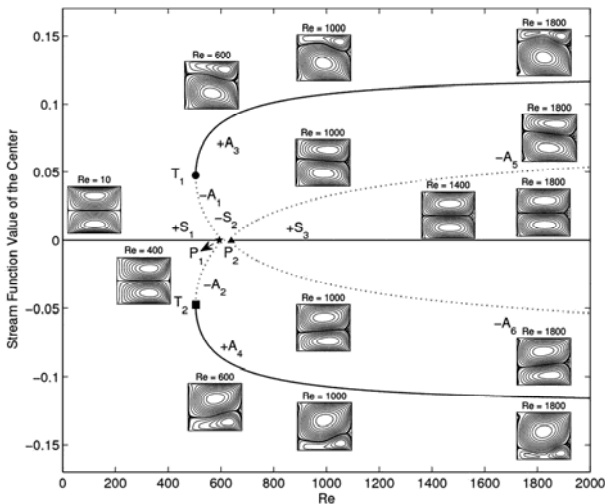


Fig. 4 Stream function values at the cavity center traced by the Reynolds number and the corresponding flow states for $AR = 0.877$.

in size and strength and compressed the other vortex, causing it to shrink. The asymmetry of the stable flows gradually augmented with the rising Reynolds number. When the Reynolds number exceeded 600, two small secondary vortices formed near the center of the right wall. With the increase in the Reynolds number, the strength of the two secondary vortices gradually increased, which resulted in the shrinkage of the two primary vortices in size.

The third type of flow bifurcation is similar to that shown in Fig. 5, which plots the value of the stream function at the cavity center as a function of the Reynolds number for a two-sided parallel lid-driven cavity flow with $AR = 0.9$. Five segments can be identified in the flow bifurcation diagram. As no pitchfork bifurcation existed in the primary branch ($+S_1$), the flow state in the branch was stable for a two vortices flow, and the strength increased as the Reynolds number increased. Furthermore, two independent branches, unconnected to the primary branch, appeared on the two sides of the primary branch, respectively. Along the two independent branches, after the turning points, T_1 and T_2 at $Re = 578$, the flow states became weak or were in a strong asymmetric state. The states ($+A_1$) and ($+A_2$) were stable, with strong asymmetric flows.

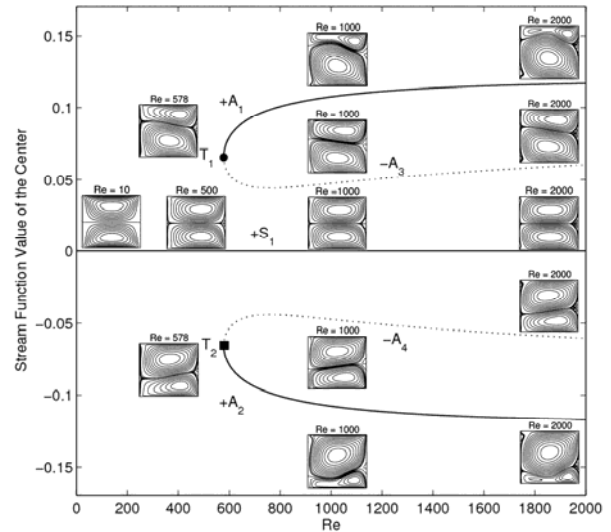


Fig. 5 Stream function values at the cavity center traced by the Reynolds number and the corresponding flow states for the case with $AR = 0.9$.

However, states ($-A_3$) and ($-A_4$) were unstable and had weak asymmetric flows. The asymmetry of the stable flows gradually augmented with the rising Reynolds number.

3.2 Evolution of Flow Bifurcations with the Increased Aspect Ratio

When the aspect ratios were less than 0.544, no asymmetric flow state existed under the range of the Reynolds numbers considered. Figure 6 illustrates the evolution of the flow bifurcations for the cases with AR in the range of 0.544 to 0.82. In this range, the solution path for the asymmetric flow pattern formed a closed loop; it meant that, with the increase in Reynolds number, the asymmetry of the asymmetric flow was gradually augmented at first and then decreased until symmetry was regained. The type of the flow bifurcations in the range is similar to that of Fig. 2. As AR increased, the value of the Reynolds number at the first pitchfork bifurcation, P_1 , gradually decreased; however, the value of the Reynolds number at the second pitchfork bifurcation, P_2 , gradually increased. Thus, the range of the closed loop and the existent region of the stable asymmetric flow also gradually enlarged with the increased aspect ratio.

Figure 7 illustrates the bifurcation diagram for the cases with AR between 0.823 and 0.87715. For the cases with aspect ratios greater than 0.82, another pitchfork bifurcation, P_2 , could be found at higher Reynolds numbers. With the increased aspect ratio, via the bifurcation point, three different flow solutions, ($-A_5$), ($-A_6$) and ($+S_3$), were found in the range of Reynolds numbers investigated. The type of the flow bifurcations in the range is similar to that of Fig. 4. For the cases with AR less than 0.86, both asymmetric flow solutions ($+A_1$) and ($+A_2$) via bifurcation point P_1 were stable. However, for the cases with AR greater than 0.86, the asymmetric flow via bifurcation point P_1

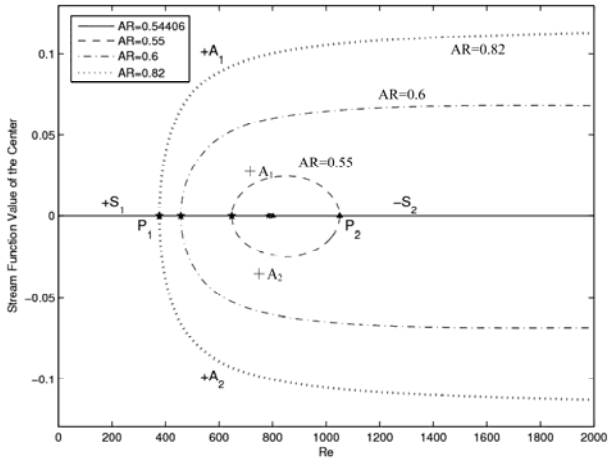


Fig. 6 Stream function values at the cavity center traced by Re for parallel motion with AR between 0.544 and 0.82.

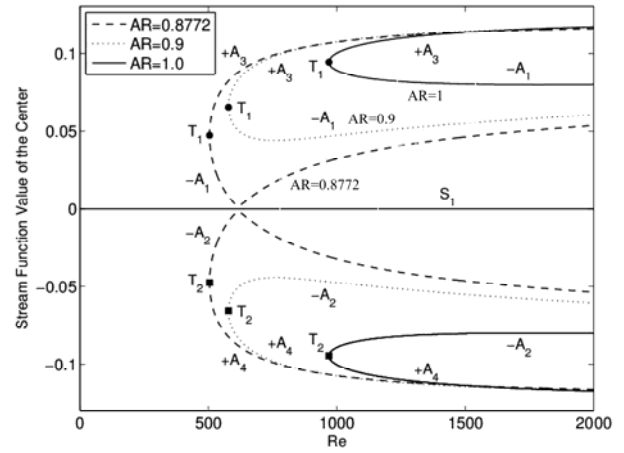


Fig. 8 Evolution of flow bifurcations for cases with aspect ratios between 0.8772 and 1.

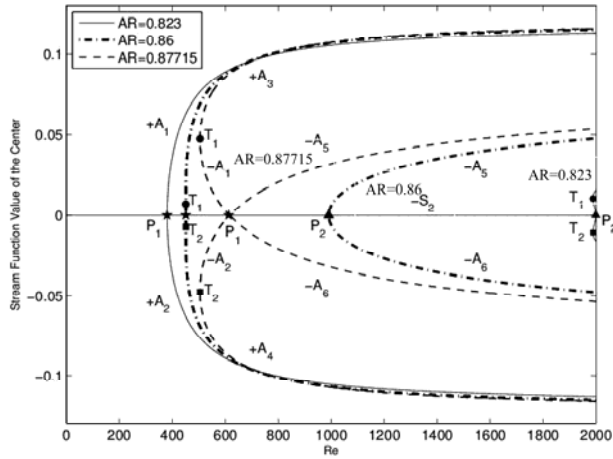


Fig. 7 Evolution of the flow bifurcations for the cases with aspect ratios between 0.823 and 0.87715.

became unstable and then stabilized via two turning points, T_1 and T_2 , respectively. With the increase in AR, the Reynolds number of the pitchfork bifurcation, P_2 , gradually decreased, and the distance between bifurcation points P_1 and P_2 was gradually reduced. The symmetric flow solution, $-S_2$, between P_1 and P_2 was unstable. For the case with AR equal to 0.877, the two pitchfork bifurcations, P_1 and P_2 , overlapped.

Figure 8 illustrates the bifurcation diagram for the cases with AR greater than 0.8772 and less than 1. The difference between Figures 7 and 8 is obvious. In Fig. 7 there are two pitchfork bifurcation points, while in Fig. 8 the two bifurcation points “collide” and disappear. As AR increased, the asymmetry of the stable asymmetric flow was gradually augmented, and the Reynolds numbers of the turning points, T_1 and T_2 , also gradually increased. Thus, the margin of the region of the stable asymmetric flow also increased in regard to the Reynolds number. The type of the flow bifurcations in the range is similar to that of Fig. 5. It should be noted that, in the aspect ratio range investigated, the stable symmetric flow state existed in the full range of Reynolds number investigated.

Figure 9 shows the regions of Reynolds numbers for all stable flow states with the increase in AR. For an AR less than 0.544, a stable symmetric flow state could be found in the full region of aspect ratios investigated, but the asymmetric flow state did not exist in the region. When the AR ranged between 0.55 and 0.585, the region of the asymmetric flow gradually augmented in a high Reynolds number region. However, a stable symmetric flow was only found in the region of a small Reynolds number. For the case with AR equal to 0.75, at the lowest Reynolds number, $Re = 350$, an asymmetric flow could be observed. When the aspect ratio was greater than 0.823, a stable symmetric flow could again be found in a high Reynolds number region. Then, with the increased aspect ratio, the critical Reynolds number of the symmetric flow gradually decreased. When the aspect ratio was equal to 0.87715, a stable symmetric flow state could be found in the full region of Reynolds numbers investigated. Table 1 lists detailed information on the values of Reynolds numbers at the pitchfork bifurcation points.

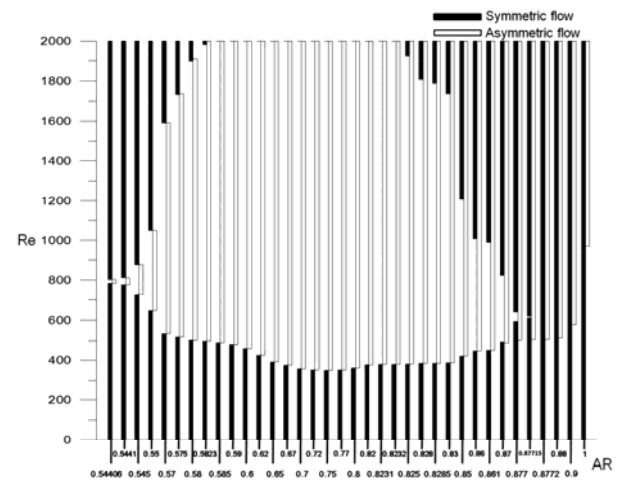


Fig. 9 Existing ranges of stable symmetric and asymmetric flow states in Reynolds numbers and aspect ratios investigated.

Table 1 Corresponding Reynolds number of bifurcation points with various aspect ratios for parallel motion.

| Aspect ratio (AR) | P_1 | P_2 | $T_1 (T_2)$ |
|-------------------|--------|---------|-------------|
| 0.544 | 785.1 | 802.4 | – |
| 0.545 | 727.54 | 876.53 | – |
| 0.55 | 647.6 | 1050.71 | – |
| 0.57 | 535.37 | 1590.06 | – |
| 0.575 | 518.5 | 1734.63 | – |
| 0.58 | 503.7 | 1897.5 | 1909.4 |
| 0.5823 | 497.43 | 1982.01 | 1779.8 |
| 0.585 | 490.4 | – | 1870.92 |
| 0.59 | 478.5 | – | – |
| 0.6 | 457.6 | – | – |
| 0.62 | 424.9 | – | – |
| 0.65 | 390.8 | – | – |
| 0.67 | 375.0 | – | – |
| 0.7 | 359.09 | – | – |
| 0.72 | 352.86 | – | – |
| 0.75 | 349.68 | – | – |
| 0.77 | 351.81 | – | – |
| 0.8 | 361.57 | – | – |
| 0.82 | 377.29 | – | – |
| 0.8232 | 380.41 | 1998.9 | – |
| 0.825 | 382.23 | 1923.73 | – |
| 0.828 | 385.5 | 1808.24 | – |
| 0.83 | 387.84 | 1737.29 | – |
| 0.85 | 420.31 | 1205.37 | – |
| 0.86 | 447.35 | 1009.04 | – |
| 0.861 | 450.79 | 990.5 | 450.78 |
| 0.877 | 594.21 | 640.95 | 504.02 |
| 0.87715 | 612.8 | 620.36 | 504.5 |
| 0.88 | – | – | 513.74 |
| 0.9 | – | – | 578.28 |
| 1.0 | – | – | 969.35 |
| 1.1 | – | – | 1742.81 |
| 1.12 | – | – | 1956.04 |
| 1.124 | – | – | 2002.51 |

4. CONCLUSIONS

This study has presented a continuation method to calculate flow bifurcation in a two-sided lid-driven cavity with different aspect ratios ($0.5 \leq AR \leq 1$) for parallel motion. Comprehensive bifurcation diagrams of the cavity flows with different aspect ratios of the cavities were derived via Keller's continuation method and accompanied with a linear stability analysis to identify the nature of the various flow solutions. The Reynolds number ($1 \leq Re \leq 2000$) was used as the continuation parameter to trace the solution curves. When $AR = 0.54$, two symmetry-breaking points were identified, and between the two points there were only asymmetric solutions in the region of the Reynolds numbers.

The evolution of the bifurcation diagrams in cases with different aspect ratios has been illustrated. The three different types of bifurcation diagrams and their corresponding flow states were classified according to

the aspect ratios. In the bifurcation diagrams, one stable symmetric flow and one stable asymmetric flow were identified, and the regions of the stable flows in the aspect ratios and Reynolds numbers were distinguished. The stable asymmetric flow state could be obtained at an aspect ratio ranging from 0.54 to 1 and at a low Reynolds number. In cases with the aspect ratio less than 0.54, only a symmetric stable two-vortex flow state existed in the bifurcation diagrams without any bifurcation branch for $0 < Re < 2000$. Furthermore, from the evolutions of the bifurcation diagrams, with the increase in the aspect ratio, the corresponding Reynolds numbers of turning points, T_1 and T_2 , also gradually increase. Therefore, it could be speculated that, there exists a critical value of aspect ratio. While the aspect ratio is greater than 0.54 but less than the critical value, the asymmetric stable two-vortex flow would exist for Reynolds numbers from 0 to 2000. The results will prove useful for designers who will be able to obtain specific flow states by adjusting the moving speed of the walls in practical experiments.

ACKNOWLEDGEMENTS

The author gratefully acknowledges the financial support provided by the National Science Council of Taiwan under Grant Nos. NSC 101-2622-E-167-019-CC3 and NSC 101-2221-E-167-010 for this study.

REFERENCES

1. Pan, F. and Acrivos, A., "Steady Flows in Rectangular Cavities," *Journal of Fluid Mechanics*, **28**, pp. 643–655 (1967).
2. Prasad, A. K. and Koseff, J. R., "Reynolds Number and End-Wall Effects on a Lid-Driven Cavity Flow," *Physics of Fluids A*, **1**, pp. 208–218 (1989).
3. Ahlman, D., Söderlund, F., Jackson, J., Kurdila, A. and Shyy, W., "Proper Orthogonal Decomposition for Time-Dependent Lid-Driven Cavity Flows," *Numerical Heat Transfer Part B-Fundamentals*, **42**, pp. 285–306 (2002).
4. Croce, G., Comini, G. and Shyy, W., "Incompressible Flow and Heat Transfer Computations Using a Continuous Pressure Equation and Nonstaggered Grids," *Numerical Heat Transfer Part B-Fundamentals*, **38**, pp. 291–307 (2000).
5. Kuhlmann, H. C., Wanschura, M. and Rath, H. J., "Flow in Two-Sided Lid-Driven Cavities: Non-Uniqueness, Instabilities, and Cellular Structures," *Journal of Fluid Mechanics*, **336**, pp. 267–299 (1997).
6. Kuhlmann, H. C., Wanschura, M. H. and Rath, J., "Elliptic Instability in Two-Sided Lid-Driven Cavity Flow," *European Journal of Mechanics B/Fluids*, **17**, pp. 561–569 (1998).
7. Albensoeder, S., Kuhlmann, H. C. and Rath, H. J.,

- “Multiplicity of Steady Two Dimensional Flows in Two-Sided Lid-Driven Cavities,” *Theoretical and Computational Fluid Dynamics*, **14**, pp. 223–241 (2001).
8. Alleborn, N., Raszillier, H. and Durst, F., “Lid-Driven Cavity with Heat and Mass Transport,” *International Journal of Heat and Mass Transfer*, **42**, pp. 833–853 (1999).
 9. Albensoeder, S. and Kuhlmann, H. C., “Linear Stability of Rectangular Cavity Flows Driven by Anti-Parallel Motion of Two Facing Walls,” *Journal of Fluid Mechanics*, **458**, pp. 153–180 (2002).
 10. Blohm, C. and Kuhlmann, H. C., “The Two-Sided Lid-Driven Cavity: Experiments on Stationary and Time-Dependent Flows,” *Journal of Fluid Mechanics*, **450**, pp. 67–95 (2002).
 11. Yang, R. J. and Luo, W. J., “Multiple Fluid Flow and Heat Transfer Solutions in a Two-Sided Lid-Driven Cavity,” *International Journal of Heat and Mass Transfer*, **50**, pp. 2394–2405 (2007).
 12. Albensoeder, S. and Kuhlmann, H. C., “Three-Dimensional Instability of Two Counter Rotating Vortices in a Rectangular Cavity Driven by Parallel Wall Motion,” *European Journal of Mechanics B/Fluids*, **21**, pp. 307–316 (2002).
 13. Chen, K. T., Tsai, C. C., Luo, W. J. and Chen, C. N., “Multiplicity of Steady Solutions in a Two-Sided Lid-Driven Cavity with Different Aspect Ratios,” *Theoretical and Computational Fluid Dynamics*, **27**, pp. 767–776 (2013).
 14. Cadou, J. M., Guevel, Y. and Girault, G., “Numerical Tools for the Stability Analysis of 2D Flows: Application to the Two- and Four-Sided Lid-Driven Cavity,” *Fluid Dynamics Research*, **44**, pp. 031403 (2012).
 15. Waheed, M. A., “Mixed Convective Heat Transfer in Rectangular Enclosures Driven by a Continuously Moving Horizontal Plate,” *International Journal of Heat and Mass Transfer*, **52**, pp. 5055–5063 (2009).
 16. Noor, D. Z., Kanna, P. R. and Chern, M. J., “Flow and Heat Transfer in a Driven Square Cavity with Double-Sided Oscillating Lids in Anti-Phase,” *International Journal of Heat and Mass Transfer*, **52**, pp. 3009–3023 (2009).
 17. Keller, H. B., *Numerical Solution of Bifurcation and Nonlinear Eigenvalue Problems, In applications of Bifurcation Theory*, P. Rabinowitz Ed., Academic Press, New York, pp. 359–384 (1977).
 18. Sorensen, D. C., “Implicit Application of Polynomial Filters in a K-Step Arnoldi Method,” *SIAM Journal of Matrix Analysis and Applications*, **13**, pp. 357–367 (1992).
 19. Saad, Y., *Numerical Methods for Large Eigenvalues Problems*, Halsted Press, New York (1992).
 20. Yang, R. J. and Luo, W. J., “Flow Bifurcations in a Thin Gap Between Two Rotating Spheres,” *Theoretical and Computational Fluid Dynamics*, **16**, pp. 115–131 (2002).
 21. Luo, W. J., Yarn K. F. and Hsu, S. P. “Analysis of Electrokinetic Mixing Using AC Electric Field and Patchwise Surface Heterogeneities,” *Japan Journal of Applied Physics*, **46**, pp. 1608–1616 (2007).

(Manuscript received December 10, 2013, accepted for publication March 13, 2014.)